South African Journal of Chemical Engineering 45 (2023) 210–220

Contents lists available at ScienceDirect

South African Journal of Chemical Engineering

journal homepage: www.elsevier.com/locate/sajce

An analysis of the processes, kinetics and equilibrium of iron's biosorption on immobilized green microalgae

P.P. Diale [a,*], D. Hildebrandt [b], D. Glasser [c], T.S. Matambo [c], S.S. Makgato [d]

[a] University of the Witwatersrand, School of Chemical and Metallurgical Engineering, Private Bag 3, Wits 2050, South Africa
[b] African Leadership Centre, WITS Business School, Molecular Science Institute, School of Chemistry, University of the Witwatersrand, Johannesburg, 2050, South Africa
[c] Institute for the Development of Energy for African Sustainability (IDEAS), University of South Africa, College of Science, Engineering and Technology, Florida, Roodepoort, 1709, South Africa
[d] Department of Chemical Engineering, College of Science, Engineering and Technology, University of South Africa (UNISA), c/o Christiaan de Wet & Pioneer Avenue, Florida Campus 1710, Johannesburg, South Africa

ARTICLE INFO

Keywords:
Biosorption
Ca-alginate
Desmodesmus sp.
Remediation
Iron

ABSTRACT

Metals including Cu, Cd, Ni, Pb, Zn, Hg, Fe and Cr can be found in significant concentrations in acid mine drainage effluent from previous gold mining operations. Even at very low levels, heavy metals and their compounds are very toxic, carcinogenic, mutagenic and teratogenic. Acid mine drainage discharge must therefore be properly treated before disposal. In this study, iron removal from acid mine drainage effluent using immobilized green microalgae is explored. The impact of pH on iron metal concentrations was studied at multiple pH values between 2 and 12 using 0.1 M HCl or NaOH solutions. At pH 6, the optimal value, 82% and 90% of Fe (II) were removed from Ca-alginate beads and immobilized *Desmodesmus sp*., respectively. It was shown that Fe (II) ions were biosorbed by immobilized microalgae cells in a pseudo-second-order manner. This study demonstrated how immobilized green microalgae showed potential to remove iron from acid mine drainage effluent.

1. Introduction

Since the Republic of South Africa has operated gold mines for over 130 years, acid mine drainage (AMD) contamination has led to the widespread discharge of metal species. Some examples of the physical, chemical and biological factors that affect AMD formation include pyrite weathering chemistry, microbiological controls, the depositional environment, the acid/base balance of the overburden, lithology, mineralogy and the hydrological conditions at the mine site (Akpan et al., 2021). Hydrochemical reactions between gold seams and groundwater produce hydrogen ions and heavy metals ions like manganese and iron, which acidify groundwater globally. Iron persists in nature and causes bioaccumulation in the food chain due to its indestructibility and lack of biodegradability, which has adverse effects on both the environment and people (Leong and Chang, 2020; Abidli et al., 2022). Despite their very low concentrations, these heavy metals and their compounds are mutagenic (Fu and Xi, 2020), carcinogenic (Boudebbouz et al., 2021) and teratogenic (Kumar et al., 2015). According to some studies, exposure to these heavy metals through direct touch, inhalation and ingestion pose serious concerns to the overall ecosystem(Abidli et al., 2022), physical and mental well-being of people by generating genetic harm and mutations that can affect the central nervous system (Briffa et al., 2020) and raise the risk of cancer (Leong and Chang, 2020). Maree et al. (2004) estimated that South Africa's Gauteng province would need to neutralize 240 ML of acid mine water per day at a cost of around $3,5 million per year. Thus, wastewater containing these heavy metals and compounds must be treated using sustainable, cost-effective and environmentally friendly remediation technologies.

Some well-known methods for treating AMD include the precipitation of chemicals (Fu and Wang, 2011), exchange of ions (Bashir et al., 2019), floatation (Fu and Wang, 2011), coagulation-flocculation (Leong and Chang, 2020), electrochemical (Alcolea et al., 2012) and membrane separation (Abdullahet et al., 2019). However, these conventional methods are only partially effective, especially when the solution has metal concentrations between 1.0 and 10 mgL^{-1} (Taylor et al., 2005) which can also lead to secondary pollution through the creation of hazardous sludge (Genty et al., 2012). It has been proven that precipitation is ineffective in AMD treatment, as it is unable to produce desired final water quality for release into the environment (Seath and van Niekerk, 2011). Generally, traditional heavy metal removal technologies (such as ion exchange or lime precipitation) are very ineffective

* Corresponding author.
E-mail address: pdiale305@gmail.com (P.P. Diale).

https://doi.org/10.1016/j.sajce.2023.05.007
Received 10 September 2022; Received in revised form 10 April 2023; Accepted 25 May 2023
Available online 26 May 2023

Nomenclature

C_0	The initial concentration (mg/L)
C_e	The equilibrium concentration (mg/L)
V	The volume of aqueous solution (L)
m	The mass of the biosorbent (g)
C_t	The iron concentration at time t (mg/L)
Ce	The equilibrium concentration of adsorbate (mg/L^{-1})
Q_e	The amount of metal adsorbed per gram of the adsorbent at equilibrium (mg/g)
Q_{max}	The maximum monolayer coverage capacity (mg/g)
K_L	The Langmuir isotherm constant (L/mg)
q_e	The sorption capacities at equilibrium (mg/g)
q_t	The sorption capacities at time *t*, respectively (mg/g)
k_1	The rate constant of first order sorption (1 / min).
Q_e	The adsorption on the adsorbent at equilibrium
C_{Fe}^{∞}	Equilibrium concentrations of Fe (II) solution (mg/L)
C_{Fe}^{0}	Initial concentrations of Fe (II) solution (mg/L)
k_r	Rate constant for the reverse reaction
k_f	Rate constant for the forward reaction
N_0^{∞}	Initial number of binding sites
N_e^{∞}	Number of binding sites at equilibrium
N_T	Total number of binding sites
V	Volume of Fe (II) ion solution.

and/or very expensive, especially when other impurities (Birungi and Chirwa, Birungi and Chirwa, 2015) and contaminants in wastewater effluents interfere with the recovery process (Abidli et al., 2022). Additionally, their applications are limited by the need for a large quantity of limestone, low efficacy and the inability to remove all metals/metalloids (Jaafari and Yaghmaeian, 2019). This necessitates the creation of cutting-edge technologies for heavy metal cleanup and removal. Thus, an economical, affordable and effective remediation technology should be able to effectively reduce heavy metal concentrations to environmentally acceptable levels as well as apply to field conditions such as effluents and aquatic bodies.

Bhatt et al. (2022) stated that bacteria, fungi and algae are frequently utilized to eliminate contaminants in biological treatment. According to Priyadarshani et al. (2011), algae accumulate toxic heavy metals from the surrounding environment at a higher concentration than those in the surrounding water. Many scientists throughout the world have emphasized the benefits of using microalgae for metal biosorption. Benefits include the ability to swiftly absorb metal, time and energy savings, environmental friendliness and user-friendliness (Kumar et al., 2015). The biological techniques can remove heavy metals from diluted solutions and regenerate the environmentally compliant solution at a cheap cost and great efficiency. In some cases, they might also provide metal recovery. The use of bacteria, microalgae, yeasts and fungus in heavy metal bioremediation has gained favor recently as an alternative to conventional methods (Leong and Chang, 2020). Microalgae are superior to all other microbes in terms of their biological traits, for instance, their high photosynthetic efficiency and easy structure, they can endure harsh circumstances in the environment such as the presence of heavy metals, high salinity, nutritional stress and extreme temperatures (Maqsood et al., 2022). As a result, microalgae's contribution to AMD goes beyond merely adjusting pH levels and actively removing heavy metal concentrations from contaminated water streams to also include preventing the production of dangerous sludge.

The algae use the pollutants as their sole source of nutrition and energy for their growth and to produce biomass (Bhatt et al. (2022). Metal ions are removed through a process called "biosorption," which involves both adsorption and absorption. According to several authors, microalgae use a process called biosorption, which is a passive, active transport mechanisms and metabolic-independent process to remove heavy metals from aqueous solutions (Makhanya et al., 2021; Wong and Tam, 1998). Rugnini et al. (2018) reported that green microalgae can be used to remove nitrogen and phosphorus from wastewater through a process called "assimilation." The majority of studies on heavy metals and microalgae focused on Cr, Cu, Hg, Zn, Pb, Ni and Cd (Kumar et al., 2015). Microalgae have also been tested for heavy metal adsorption at low pH (1–6.0) and concentrations several times greater and lower than AMD wastewater (Makhanya et al., 2021). Although microalgae offer several advantages, more research is needed to see whether it is possible to use them to remove additional dominant heavy metal concentrations associated with AMD, which has not been studied. This study focuses on the removal of iron from AMD effluent by immobilized green microalgae.

2. Materials and methods

2.1. Simulated water

A water sample from a point source of AMD effluent from previous gold mining operations was examined in detail. The total iron content at the time of sampling was 998 mg/L. A hydrated metal salt of $FeSO_4{\cdot}7H_2O$ of analytical grade (Sigma-Aldrich, South Africa) was made into a 1000 mg/L stock solution of Fe (II) ions and dissolved in deionized water. To achieve a pH of 2.5, sulphuric acid (H_2SO_4) (90–99%) was utilized. The aforementioned stock standard solution was appropriately diluted to create the necessary beginning concentrations.

2.2. Microalgae community analysis

Donaldson Dam, one of the water bodies in the West Witwatersrand basin that are impacted by AMD, was sampled to determine the composition of the microalgae. Because of AMD pollution, the dam has previously documented an alarming amount of fish deaths. Using the standard cetyl trimethylammonium bromide (CTAB) extraction procedure, a highly mixed microalga sequence was extracted from the dam and used directly for Polymerase Chain Reaction (PCR) amplification. To identify the unidentified algal sample, the internal transcriber region (ITS2) was amplified. The PCR settings were 1 KAPA Robust Mix (KAPA), 0.5 M of each primer, and 20 ng DNA. In an Applied Biosystems Veriti Thermal Cycler, the PCR was conducted under the following conditions: 95 °C for 5 min, followed by 40 cycles of 95 °C for 30 s, 50 °C for 50 s, and 72 °C for 60 s, with a final extension of 72 °C for 10 min. Purification of the PCR products was carried out using the NucleoFast Purification System (Separations). Each primer was utilized for sequencing with the BigDye Terminator V1.3 (*Applied Biosystems*), followed by electrophoresis with the 3730 × DNA Analyzer (*Applied Biosystems*).

2.3. Growth media

The modified Beijerinck medium mix was utilized to cultivate the microalgae, and it included micronutrients 1 and reagents per 1000 mL of Stock I, Stock II, and Stock III (mL). Stock I: $MgSO_4{\cdot}7H_2O$ (0.2 g), $CaCl_2{\cdot}2H_2O$ (0.2 g), NH_4NO_3 (1.5 g), and KH_2PO_4 (0.2 g) (0.1 g). Inventories II: K_2HPO_4 (9.07 g). Inventories III: K_2HPO_4 (11.61 g). EDTA (50 g), $CuSO_4{\cdot}5H_2O$ (1.5 g), $ZnSO_4.H_2O$ (22 g), $CoCl_2{\cdot}6H_2O$ (1.5 g), $FeSO_4{\cdot}7H_2O$ (5 g), and H_3BO_3 (10 g) are micronutrients (NH_4). $6Mo.7O_{24}{\cdot}4H_2O$ (1 g). The medium was prepared using only analytical-grade chemicals. The medium was autoclaved using a HA-300 MD, HICLAVE autoclave at 190 °C and 0.1 MPa. The microalgae cells were cultured in 1-liter Erlenmeyer flasks with continuous fluorescent

lighting, CO_2 bubbles once daily for an hour, and a pH of 7.

2.4. The synthesis route of calcium alginate beads

Sodium alginate was solubilized in water at 70 °C for 1 hour, yielding a 2% w/v solution. 1% w/v cellulose nanocrystals were homogenized in an Ultra-Turrax T-50 Homogenizer for 3 min. Then, a volume of sodium alginate was mixed with a volume of cellulose nanocrystal dispersion to create a solution with 1% w/v alginate and 0.05% nanocrystals. It was produced separately in 20 mM calcium chloride. To eliminate bubbles, sodium alginate and cellulose nanocrystals were placed in silicon moulds and vacuumed at −700 mmHg. A hot air oven dried the films at 45 °C for 12 h. After drying, the films were submerged in 5 mL of calcium chloride (20 mM) for 1 hour.

2.5. Environmental scanning electron microscope

An environmental scanning electron microscope was used to gather structural data on IDS at nanometre scale resolution since it can convert nonconductive samples into conductive ones without the need for desiccating and coating samples with gold-palladium or carbon. This is essential for maintaining the sample's original properties when examining biological or polymer materials like IDS since it helps preserve such properties. Samples were created and evaluated at the Council for Scientific and Industrial Research (CSIR) in Port Elizabeth, South Africa. The surface morphology of the beads was determined using the settings HV = 25 kV, Mode = SE, and Vac Mode = ESEM.

2.6. Fourier transform infrared spectra

FTIR spectra between 400 and 4000 cm^{-1} were recorded using a Bruker FTIR spectrometer, Model Tensor 27 (Ettlingen, Germany). The solid state was used to record the spectra. The technique was applied to investigate the IDS and CB's properties both before and after their interaction with the Fe (II) ion solution. The FTIR spectrum was used as a fingerprint for identification by contrasting the "unknown" item's spectrum with documented reference spectra.

2.7. Effect of pH on metal uptake

One of the major factors influencing the biosorption process is pH, which has an impact on the sorbates' level of ionization and speciation as well as the sorbent material's surface charge (Santaeufemia et al., 2021). It was carried out to examine the impact of IDS and CB on metal adsorption. 50 mL of an artificial solution with 120 ppm Fe^{2+} were added to Erlenmeyer flasks. The flasks were filled with 5 g and 3 mm of IDS and CB biomass, respectively, and the mixture was stirred with the metal solution for 120 min at 180 rpm. The solution was filtered, the pH value was established, and the liquid supernatant's metal content on the inductively coupled plasma was evaluated (ICP-OES).

2.8. Batch biosorption study

Batch sorption studies were conducted using six 250 mL Erlenmeyer flasks that contained 5 g of IDS in 50 mL of a 120 mg/L Fe (II) solution at pH 2.5. IDS and CB were added to each flask, which was then allowed to shake in a solution of Fe (II) while being continuously stirred at 180 rpm using an orbital shaker (MRC Scientific Instruments, UK). Samples were drawn from flasks at intervals of 5, 10, 15, 30, 60 and 120 min. After passing the gathered solution through a Whatman cellulose nitrate membrane filter (0.45 m), which has a 47 mm diameter, beads were separated from the supernatant.

2.9. Analysis of heavy metals in aqueous solutions concentration

End-on-plasma ICP-OES from Spectro Genesis The quantity of Fe (II) ions present in filtrates was determined using Spectro Analytical Instruments (Pty) Ltd, (Johannesburg, South Africa). Q_e (mg metal / g alga) (mg/g) is a mathematical expression that represents the quantity of Fe (II) ions that are sorbed per unit of biomass. This was determined using the mass balance's Eq. (1), as follows:

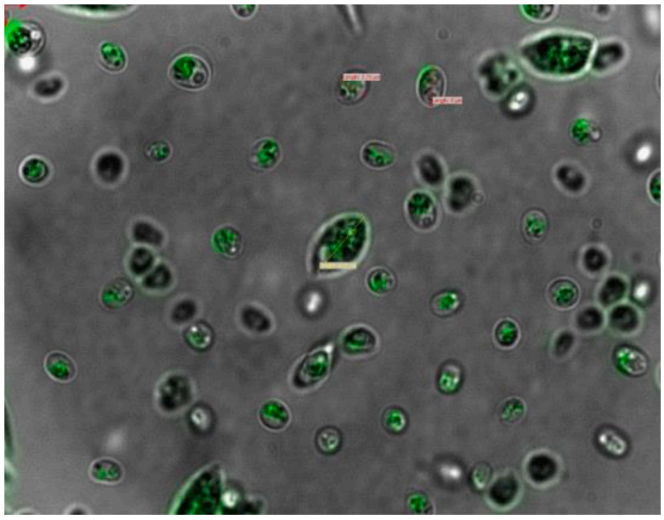

Fig. 1. Image of algae found in the sample.

$$Q_e = \frac{(C_0 - C_e)V}{m} \quad (1)$$

where: C_0 is the initial concentration (mg/L), C_e is the equilibrium concentration (mg/L), V is the volume of aqueous solution (L) and m is the mass (g) of the biosorbent. A control experiment using CB was also carried out. The performance of the IDS and CB sorption were evaluated using removal efficiency RE (%) as indicated in Eq. (2):

$$RE\ (\%) = \frac{C_{0-}\ C_t}{C_0} \text{x } 100 \quad (2)$$

where: C_t is the iron concentration at time t (mg/L) and C_0 the initial concentration (mg/L).

2.10. Point of zero charge (pH_{pzc})

We calculated the point of zero charge (pHpzc) for CB and IDS using the solid addition method. This is the pH level at which a surface charge is equal to zero. pH would be either increased or decreased based on this to make the surface more negative or positive. The pHpzc was determined by measuring the pH after adding 50 mL of a 0.01 M $NaCl_2$ solution to six sealed Erlenmeyer flasks. The solutions were raised to starting pHs of 2, 4, 6, 8, 10 and 12 using 0.1 M HCl or NaOH solutions. Immobilized alginate beads weighing 0.15 g were added to each solution, which was then agitated vigorously for 48 h at 25 °C. The final pH values of each solution were then measured in the liquid supernatant after filtering. The pH_{pzc} is obtained by plotting a pH_{final} vs. $pH_{initial}$ curve. Using $pH_{initial} = pH_{final}$ as the point of intersection, a straight line was drawn from the origin to the pH_{pzc} of the beads.

3. Results and discussions

3.1. Microalgae community analysis

The internal transcriber region (ITS2) was amplified to identify the unknown algal sample and a single product was observed. A highly mixed sequence was obtained and was used as is. The sequences were checked against the internal transcriber spacer 2 database and NCBI (Schultz et al., 2006). Fig. 1 depicts an image of algae found in the

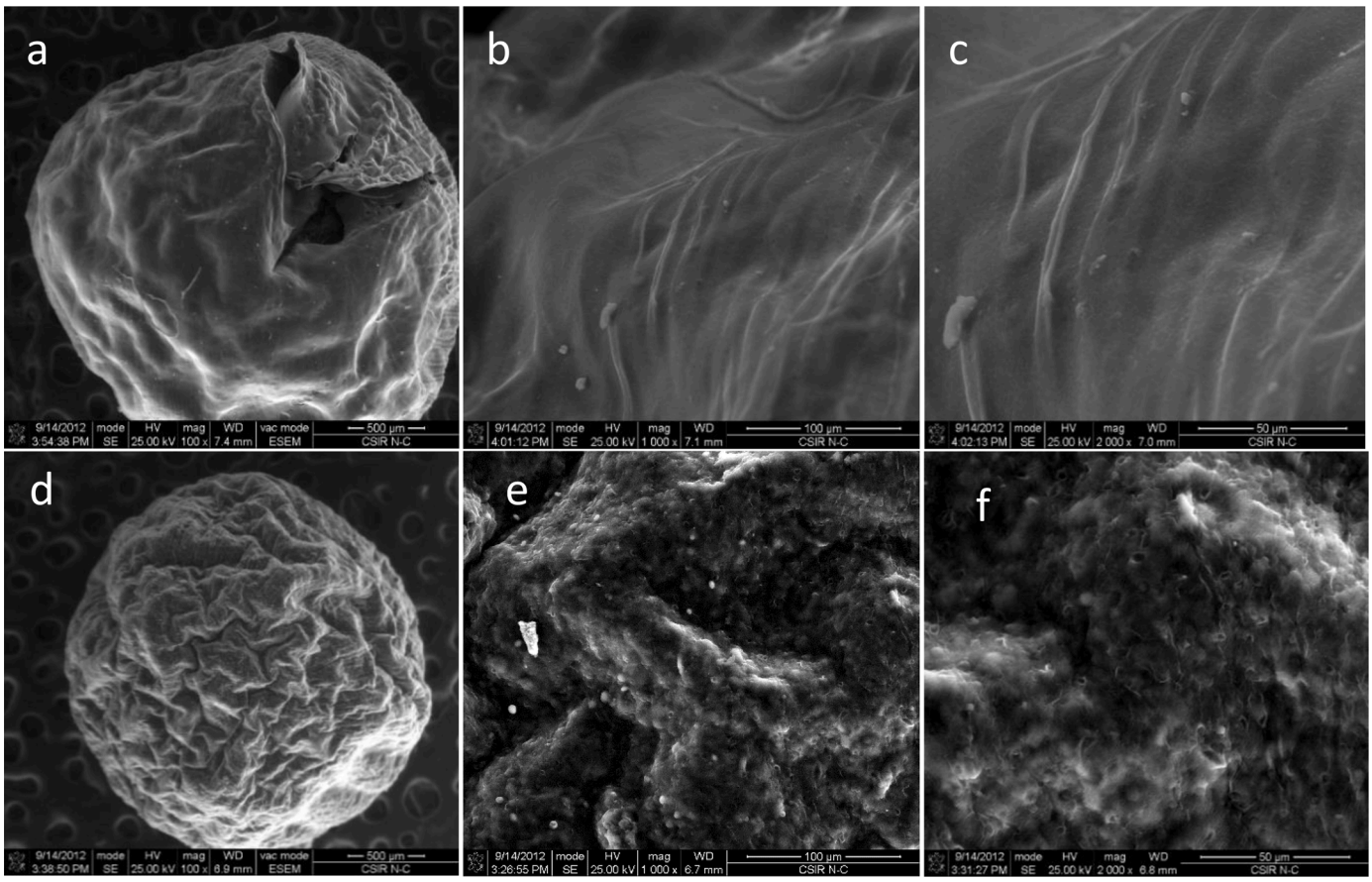

Fig. 2. Surface topography by ESEM of CB: (a - c) Mag = 100 ×, WD = 7.4 mm, 500 μm; Mag = 1000 ×, WD = 7.1 mm, 100 μm and Mag = 2000 ×, WD = 7.0 mm, 50 μm. Surface topography by ESEM of IDS: (d - f) Mag = 100 ×, WD = 6.9 mm, 500 μm; Mag = 1000 ×, WD = 6.7 mm, 100 μm and Mag = 2000 x, WD = 6.8 mm, 50 μm.

sample.

An F-view-II cooled CCD camera connected to an IX-81 inverted fluorescence microscope with an Olympus Cell R system was used to view the samples (Soft Imaging Systems). Pictures were taken using an Olympus Biosystems GMBH Xenon-Arc burner and a 472 nm excitation filter as the light source. Emission was recorded with a UBG triple-

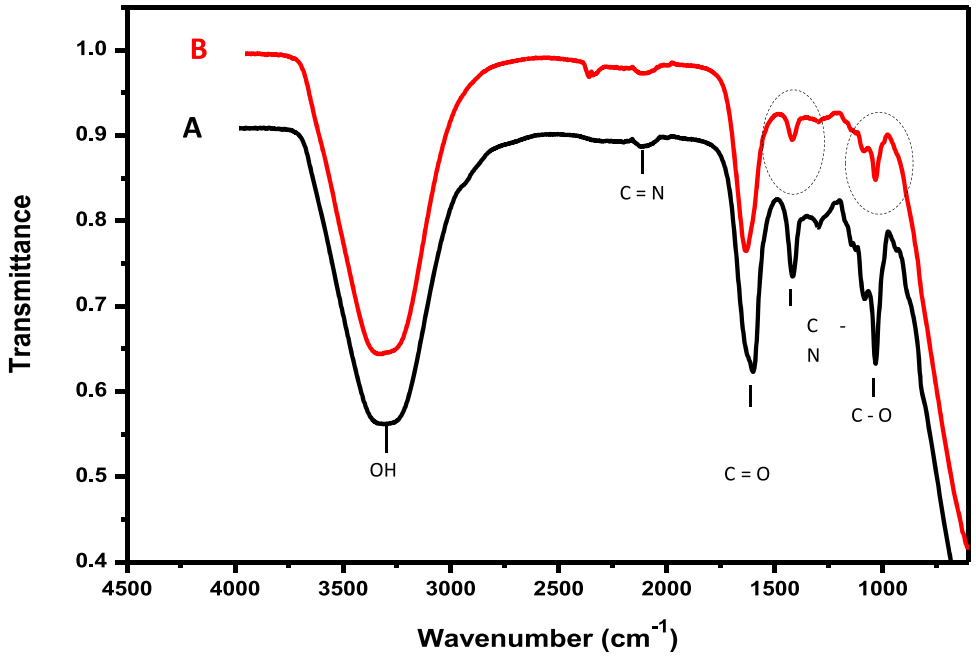

Fig. 3. The FTIR spectra of (A) IDS before Fe (II) biosorption and (B) after Fe (II) biosorption.

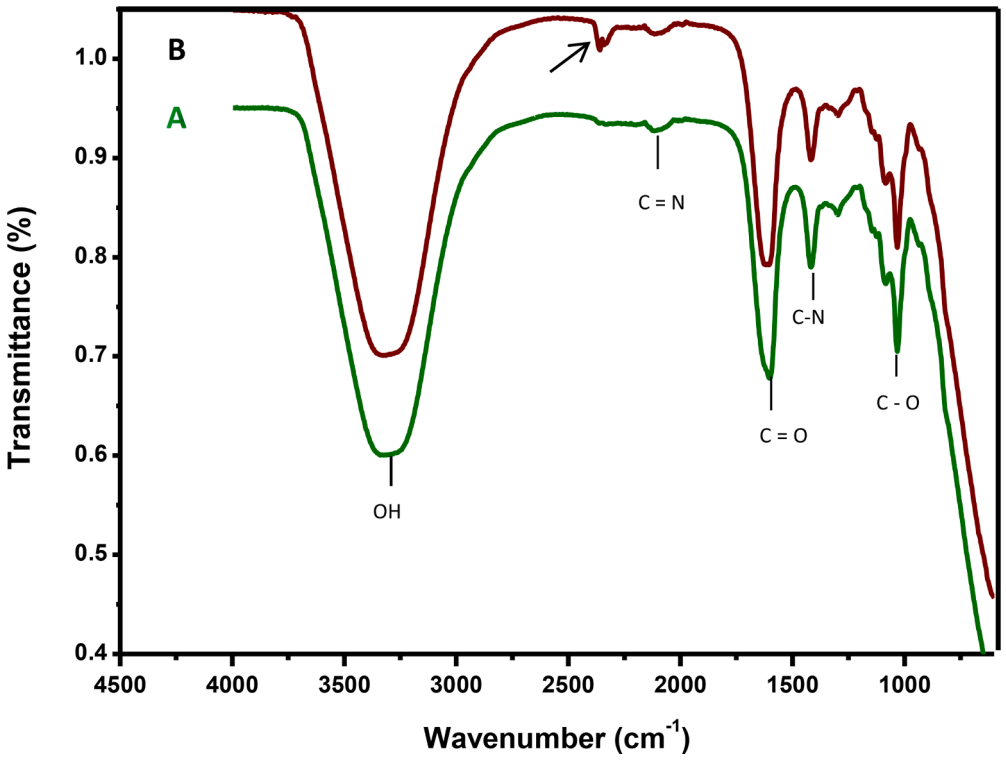

Fig. 4. The FTIR spectra of (A) CB before Fe (II) biosorption and (B) after Fe (II) biosorption.

bandpass emission filter cube (Chroma). Image acquisition was performed with an Olympus UPlan Sapo N 60 ×1.4. Images were processed and background subtracted using the CellR application. The microalgae are a green photosynthetic unicellular organism. Their green pigment is due to the presence of chlorophyll, which is found in the chloroplasts of green plants. *Desmodesmus sp.* belongs to the *Scenedesmaceae* family which has two subegnii: (i) *Scenedesmus* and (ii) *Desmodesmus* (Réka, 2014). These colonies are generally 2-, 4-, or 8-celled but rarely 16-. The cell walls of *Desmodesmus sp.* found in Donaldson dam are spineless and 2- celled. Among the microalgae species found for this study, *Desmodesmus* sp. dominated.

3.2. Characterization of immobilized microalgae

The surface structures of the IDS and CB were viewed under vacuum mode at various magnifications on an ESEM and the results are depicted in Fig. 2. As shown in Fig. 2, beads without microalgae have relatively smooth surfaces, whereas microalgal-encapsulated beads, IDS, have numerous pores. The pores on the surface of the inoculated beads can be attributed to the gel surface cracking open due to the growth of the underlying colonies (Schnee et al., 2016).

3.3. The FTIR spectra

The Fourier Transform Infrared Spectroscopy (FTIR) analyses of IDS before and after Fe (II) biosorption are depicted in Fig. 3. The circles depict how the spectra altered as a result of Fe (II) biosorption. Functional groups that played a role in Fe (II) biosorption include: -OH stretch, symmetrical alkaynes, C=O stretch, -N-H bending, symmetric CH_3 bending and -CO stretching of ester groups (Plöhn et al., 2021). The most obvious change in the spectra was noticed at bands 1604, 1421 and 1034 cm^{-1} after Fe (II) biosorption, suggesting that carboxylic, -CO stretching of ester, and -N-H bending functional groups were mainly provoked by the presence of Fe (II) ions biosorption. At a pH of 2.5, deprotonation may have caused the carboxylic group to change into carboxylate ions (Aryal and Liakopoulou-Kyriakides, 2013). According to Aryal and Liakopoulou-Kyriakides (2013), positively charged Fe $(OH)_2$ species may interact electrostatically with anions on the surface of the microalgae (Ariyal and Liakopoulou-Kyriakides, 2013). The oxygen atom's three lone pairs are responsible for the hydroxide ion's (-OH) negative charge. It can then act as a ligand for a Lewis base by transferring a lone pair from an O atom to a Fe (II) atom to establish a covalent bond. Four ligands can be coordinated and octahedrally coordinated by the potential mechanism of Fe (II) interaction with carboxylic Fe (II) atoms due to the presence of free d-orbitals in its electronic structure.

The possible structure of the compound obtained by the interaction between $Fe(OH)_2$ ion and biomass surface functional groups has been reported by Aryal and Liakopoulou-Kryriakides (2013). An overview of the interactions between the carboxyl group and Fe (II) is given by Eqs. 3 through 6.

$$R\text{-}COOH \overset{s}{\longleftrightarrow} R\text{-}COO^- + H^+ \quad (3)$$

$$2R\text{-}COO^- + Fe^{2+} + (OH)^- \overset{s}{\longleftrightarrow} (R\text{-}COO\text{-})_2\text{-}Fe(OH) \quad (4)$$

$$R\text{-}OH^- + H^+ \overset{s}{\longleftrightarrow} R\text{-}OH_2^- \quad (5)$$

$$R\text{-}OH_2^- + Fe(OH)_2 \overset{s}{\longleftrightarrow} [R\text{-}(OH)^-\text{: } Fe\ (OH_2)]_2 + H^+ \quad (6)$$

The appearance of a band at 2363 cm^{-1} after Fe (II) interaction is evidence that a coordination complex was formed. The band could represent iron enneacarbonyl ($Fe_2(CO)_9$) or iron tetracarbonyl ($Fe_3(CO)_{12}$) (Mathur et al., 1991). Mathur et al. (1991) found that the carbonyl stretching frequency of $Fe_2(CO)_9$ was at 1828 cm^{-1} while $Fe_3(CO)_{12}$ was found between 2020 – 2043 cm^{-1}. This finding implies that ion exchange and chemisorption may have taken a dominant role in the active biosorption of Fe (II) removal from aqueous solutions. According to FTIR studies, the carboxylic moieties in the cell walls are the main factor in iron removal. Abidli and collaborators employed *Scenedesmus sp.* (IMMTCC-13) for the chromium removal procedure and reported comparable outcomes (Abidli et al., 2022). On the other hand, Fig. 4 displays the FTIR spectra of CB before and after Fe (II) biosorption. Alkanes, alcohol, alkynes and carboxylic acids were also discovered to

Table 1
Initial Fe (II) concentration's impact on removal effectiveness and loading capacity when CB and IDS are present.

Substrate	Initial Fe (II) Concentration (mg/L)	Final Fe (II) concentration (mg/L)	RE (%)
Ca-alginate beads (CB	5	0.83	82
	60	19	68
	120	56	56
	240	136	43
	480	250	44
	1000	824	18
Immobilized	5	0.50	90
Desmodesmus sp.	60	11	82
(IDS)	120	48	60
	240	128	47
	480	231	52
	1000	654	35

be functional groups. In accordance with Davis et al. (2003), these functional groups were related to a variety of organic substances present in biomass, such as lipids, proteins, carbohydrates, fatty acids, nucleic acids, amino acids, cysteine and carbohydrates.

3.4. Effect of initial Fe (II) ion concentration on biosorption

The impact of the Fe (II) ion concentration at the start of the process on biosorption has been investigated. This is based on the knowledge that different contaminated water streams have different metal ion concentrations, making it crucial to assess its effect during a complete biosorption analysis. The biosorbent loading capacity and RE% of Fe (II) from aqueous solutions are shown in Table 1 for various initial biomass concentrations IDS and CB. Aqueous solutions with a starting concentration of 5 mg/L experienced a relatively high Fe (II) removal of 82% after 120 min of biosorption. But as the Fe (II) concentration increased from 5 to 1000 mg/L, the rate of Fe (II) removal decreased from 82 to 18%. A decrease in metal removal efficiency with an increase in initial metal concentration was also observed by (Akpomie and Dawodu (2015). This implies that there is a small number of active sites in the biosorbent, and these sites become saturated at higher metal concentrations. However, with the same dose of 5 mg/L, it was discovered that RE% for IDS removal was high at 90% compared to CB at 82%. This showed that immobilization of *Desmodesmus sp* sorption increased its Fe (II) removal capabilities, and this was true at all concentrations considered. The active biosorption, which is dependent on metabolism, predominated the transfer of Fe (II) ions to the IDS surface, which may be indicative of a delayed metal binding process. Active biosorption as a mechanism for metal uptake is constituted by covalent bonding, redox reactions, crystallization on the cell surface or, most often, diffusion into the cell interior and binding to proteins and other intracellular sites (Al-Qunaibit, 2004). Pathak and Choppin (2009) suggest that the mechanism by which microalgae biomass binds metal ions depends on the species and ionic charge of metal ions, as well as the chemical composition of the metal ion solution.

3.5. The effect of pH on biosorption

Fig. 5 illustrates the impact of pH on the IDS and CB adsorption capacities. The removal percentage of CB was determined to be 56% at pH 2, which was the lowest compared to IDS's 60%. At severely acidic pH (<2), metal sorption by algae has frequently been found to decrease (Mehta and Gaur, 2001). According to Shen and Chirwa (2018), at pH levels that are severely acidic, algae have a reduced capacity to bind metals. This is because some surface functional groups cannot attach to metal due to steric hindrance (Adhiya et al., 2002). The adsorbent's surface charge may become positively charged at low pH levels, which repels the positively charged Fe (II) cations. With the highest removal effectiveness for IDS at 90% and CB at 82% for the concentration of 5 mg/L, pH 6 was the ideal pH for removing Fe (II). After pH 6, the pH did not significantly change during the experiment's time frame, and the rate of elimination of Fe (II) remained steady. According to Mehta and Gaur (2005), the functional group that demonstrated the biosorption mechanism of sequestering Fe (II) from aqueous solutions was the carboxylic functional group. This is described by how the negatively charged surface created by the acidic functional group at an acidic pH and how it interacted electrostatically with the cationic species help explain this (Monteiro et al., 2009). As the pH increases, the functional sites get deprotonated, increasing their negative charges and allowing for a higher affinity for metal cations.

3.6. Surface active site model for Fe (II) biosorption

Fig. 6 shows the response surface that reveals the combined interactive effects of Fe (II) concentration (mg/L) and absorption capacity (mg/g) of IDS as a function of time. As the initial concentration of Fe (II)

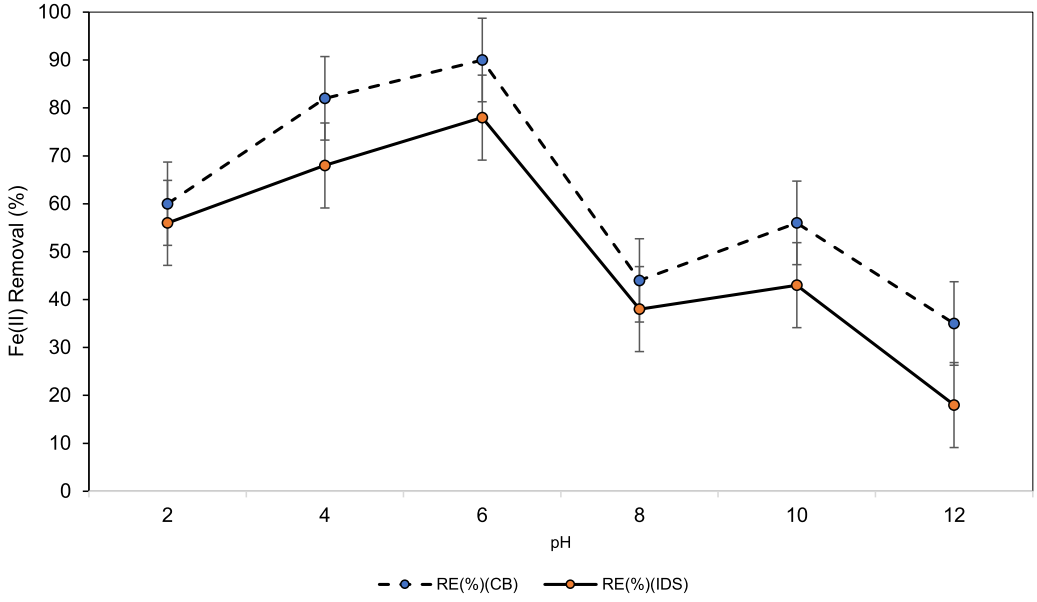

Fig. 5. The Fe (II) ion uptake at different surface pH of CB.

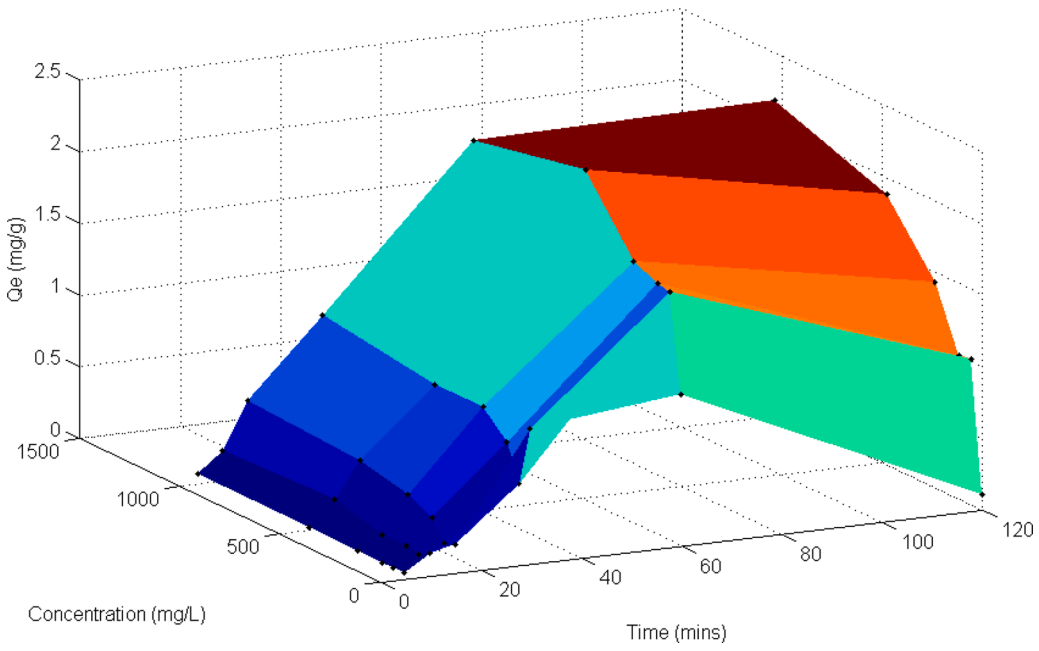

Fig. 6. Response surface revealing combined interactive effects of Fe (II) concentration (mg/L) and uptake capacity (mg/g) of IDS as a function of time.

increased, more of it was biosorbed onto the IDS. The RSM curve demonstrates the interaction between the amount of Fe (II) ions biosorbed per unit of biosorbent and the variation in starting concentration over time. As a result of electrostatic interactions between cationic species and the cell surface at an acidic pH, these groups create a negatively charged surface, which is responsible for metal biosorption (Barka et al., 2013). Using information from Fig. 6, a surface-active site model was created to estimate the potential number of binding sites. The relevant equations can be written as follows, presuming that the loading of Fe (II) ions onto the biosorbent is a reversible procedure. The forward reaction and reverse reaction on a reversible surface reaction is given by:

$$k_f C_{Fe}^{\infty} N_e^{\infty} = k_r N_0^{\infty} \tag{7}$$

the total number of binding sites is given by

$$N_T = N_e^{\infty} + N_0^{\infty} \tag{8}$$

where the initial binding sites saturation is a function of Fe (II) concentration

$$N_0^{\infty} = V\left(C_{Fe}^{0} - C_{Fe}^{\infty}\right) \tag{9}$$

to determine the number of available binding sites at equilibrium Eq. 9 is substituted into (10) so that

$$k_f C_{Fe}^{\infty}\left(N_T - N_0^{\infty}\right) = k_r N_0^{\infty} \tag{10}$$

the forward and reverse rate constants of Fe (II) ions biosorption are a

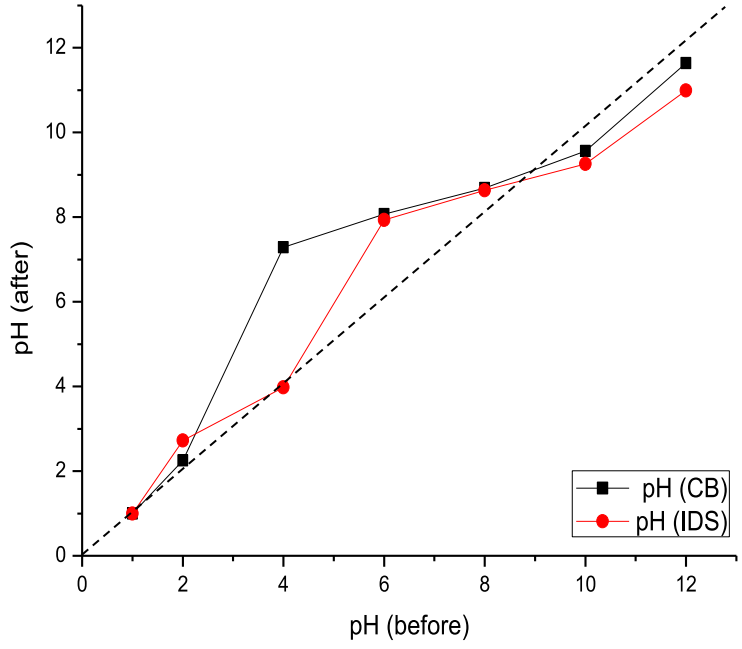

Fig. 7. The point of zero charge (pH_{pzc}) for biosorbents IDS at pH 8.8 and CB obtained at pH 9.3.

function of the initial and final metal ions available for active binding on available sites described as

$$\frac{k_f}{k_r}C_{Fe}^{\infty}N_T = N_0^{\infty} + \frac{k_f}{k_r}C_{Fe}^{\infty}N_0^{\infty} \quad (11)$$

$$\frac{k_f}{k_r}C_{Fe}^{\infty}N_T = N_0^{\infty}\left(1+\frac{k_f}{k_r}C_{Fe}^{\infty}\right) \quad (12)$$

$$\frac{k_f}{k_r}C_{Fe}^{\infty}N_T = V\left(C_{Fe}^{0} - C_{Fe}^{\infty}\right)\left(1+\frac{k_f}{k_r}C_{Fe}^{\infty}\right) \quad (13)$$

$$\left(\frac{k_f}{k_r}\right)N_T\frac{C_{Fe}^{\infty}}{V\left(C_{Fe}^{0} - C_{Fe}^{\infty}\right)} = 1+\frac{k_f}{k_r}C_{Fe}^{\infty} \quad (14)$$

The resulting kinetic equation is as follows:

$$\frac{C_{Fe}^{\infty}}{V\left(C_{Fe}^{0} - C_{Fe}^{\infty}\right)} = \left(\frac{k_r}{k_f}\right)\frac{1}{N_T} + \frac{1}{N_T}C_{Fe}^{\infty} \quad (15)$$

Where: N_0 = initial number of binding sites; Ne = number of binding sites at equilibrium; NT = total number of binding sites; V = volume of Fe (II) ion solution; C_{Fe} = equilibrium concentrations of Fe (II) solution (mg/L); C_{Fe}^0 = initial concentrations of Fe (II) solution (mg/L); k_r = rate constant for the reverse reaction; k_f = rate constant for the forward reaction.

3.7. Point of zero charge (pH_{pzc})

Since the surface charges of the biosobent samples can be verified, the pH_{pzc} aids in understanding the biosorption mechanism. The pH_{pzc} of the biosorbents IDS and CB were found to be 8.8 and 9.2, respectively, as illustrated in Fig. 7. The biosorbent's total surface charge turns positive at low pH levels (pH pH_{pzc}). This might prevent metal cations from being absorbed through the skin. The biosorbent becomes negatively charged at pH > pH_{pzc}, and a considerable metal uptake is anticipated in this range. As a result, raising the pH causes the microalgal biomass' negative charge to increase, allowing for greater electrostatic interaction between the molecules of the biomass' negative charge and the positively charged metal ions (Santaefemia and Torres, 2021). This would imply that raising pH would improve the effectiveness of Fe (II) removal by the algal biomass. At pH 8.6, the point of zero charge was identified experimentally. The charge on the beads is positive when the pH is below the iosoelectric point and negative when the pH is above the iosoelectric point. Because the total charge of the beads was negative, a remarkably high metal removal was anticipated at pH levels over the iosoelectric point. The binding of positively charged Fe (II) ions was unaffected by the surface's positive charge (pH 1–8.5). This is explained by the presence of acidic metal binding groups in the immobilized algae. The functional group carboxyl was discovered to be the dominant one. As a result of electrostatic interactions between cationic species and the cell surface at an acidic pH, these groups create a negatively charged surface, which is responsible for metal biosorption.

3.8. Biosorption isotherms

Using the Freundlich and Langmuir sorption isotherms, we examined the biosorption of Fe (II). According to Dada et al. (2012), the Langmuir sorption isotherm is predicated on the following premises: For monolayer adsorption onto surfaces with a constrained number of identical sites, the Langmuir isotherm is valid. The model assumes constant surface adsorption energies and the lack of transmigration of adsorbate. Eq. (16) uses K_L, the Langmuir constant, as the linear equation to represent the Langmuir sorption isotherm:

$$\frac{Ce}{Qe} = \frac{Ce}{q\max} + \frac{1}{K_L q\max} \quad (16)$$

Table 2
The parameters of the Freundlich and Langmuir isotherms.

Substrate	Langmuir			Freundlich		
	R^2	Q_{max} (mg/g)	K_L (L/mg)	R^2	n	K_f (L/mg)$^{1/n}$
Ca-alginate beads (CB)	0.62	0.26	0.025	0.68	0.360	12.25
Immobilized Desmodesmus sp. *(IDS)*	0.88	1.05	0.004	0.96	0.047	9.22

where Q_e is the quantity of metal adsorbed per gram of the adsorbent at equilibrium (mg/g); Ce is the equilibrium concentration of adsorbate (mg/L); K_L is the Langmuir isotherm constant (L/mg) and Q_{max} is the maximal monolayer coverage capacity (mg/g).

We investigated the biosorption of Fe using the Langmuir and Freundlich sorption isotherms (II). The following assumptions are made for the Langmuir sorption isotherm, according to Dada et al. (2012): The Langmuir isotherm holds true for monolayer adsorption onto surfaces that include a limited number of identical sites. The assumption of the model is that there is no adsorbate transmigration and that the surface adsorption energies are homogeneous. K_L, the Langmuir constant, is the linear expression used in Eq. (16) to represent the Langmuir sorption isotherm:

$$\log Qe = \log Kf + \frac{1}{n}\log Ce \quad (17)$$

where the slope and intercept of the linear Freundlich equation are equal to 1/n and log K_f, respectively, and Q_e is the equilibrium adsorption on the adsorbent. If $1/n = 1$, the Freundlich isotherm is linear; if $1/n < 1$, it is non-linear (Dada et al., 2012). The Freundlich isotherm constant is denoted by K_f.

Table 2 shows the correlation coefficients (R^2) as well as the Langmuir and Freundlich adsorption constants that were found in this experiment. It was demonstrated that the linear regression analysis by Langmuir and Freundlich offered a better match on IDS than CB. The maximal sorption absorption of Fe (II) by IDS was found to be 1.05 mg/g, whereas K_L, the coefficient relating to the affinity between the sorbent and sorbate, was found to be 0.004 L/mg in accordance with the Langmuir model. For a good biosorbent, high Q_{max} and a steep initial isotherm slope b are ideal (Wang et al., 2009; Lichtfouse et al., 2012). This demonstrated that the CB had a maximum loading capacity of 0.26 mg/g, while the IDS had a maximum loading capacity of 1.05 mg/g. It was discovered that the K_L for CB (0.004) was steeper than for IDS (0.025), indicating that CB had a somewhat higher affinity to Fe (II). To evaluate how well the model fits the biosorption process and conveys a critical aspect of the Langmuir isotherm, utilize the separation factor (R_L) (Dada et al., 2012). This dimensionless constant serves as the equation for Eq. (18).

$$R_L = \frac{1}{1+bC_0} \quad (18)$$

3.9. Biosorption kinetics of Fe (II)

The rate of solute uptake that regulates the amount of time that sorbate uptake takes place at the solid-solution interface is known as biosorption kinetics (Tarawou et al., 2010). Using pseudo-first and pseudo-second order sorption kinetic models, the rate of Fe (II) ion uptake by immobilized algal biomass was calculated. Pseudo-first-order was expressed as per Eq. (19):

$$\frac{d_{q_t}}{d_t} = k_1(q_e - q_t) \quad (19)$$

where: q_e and q_t are the sorption capacities at equilibrium and at time t, respectively (mg/g). k_1 is the rate constant of first-order sorption (1 /

Table 3
Fe (II) biosorption on immobilized microalgae beads: Pseudo-first- and Pseudo-second-order Kinetic Constants.

Substrate	Iron Concentration mg/L	Experimental Pseudo-first-order kinetics capacities Q_E (mg/g)	k_1(1/min)	Q_{eq} (mg/g)	R^2	Pseudo-second-order kinetics k_2(g/mg.min)	Q_{eq} (mg/g)	R^2
Ca-alginate beads (CB)	5	50	3.61	50	0.18	0.0042	54.16	0.99
	60	185	5.29	181	0.38	0.00058	185.86	0.98
	120	425	1.15	420	0.76	0.00029	424.26	0.98
	240	842	0.10	840	0.41	0.000145	844.55	0.99
	480	1680	0.80	1680	0.48	0.0000725	1684.20	0.99
	1000	3508	2.29	3500	0.76	0.0000344	3504.01	0.49
Immobilized Desmodesmus sp. *(IDS)*	5	95	4.27	90	0.17	0.0038	99.16	0.98
	60	225	5.95	222	0.37	0.00052	229.15	0.99
	120	475	1.81	471	0.75	0.00026	479.13	0.99
	240	895	0.76	894	0.40	0.000131	899.14	0.98
	480	1736	1.46	1733	0.46	0.0000654	1740.17	0.98
	1000	3558	2.95	3556	0.74	0.0000311	3562.16	0.48

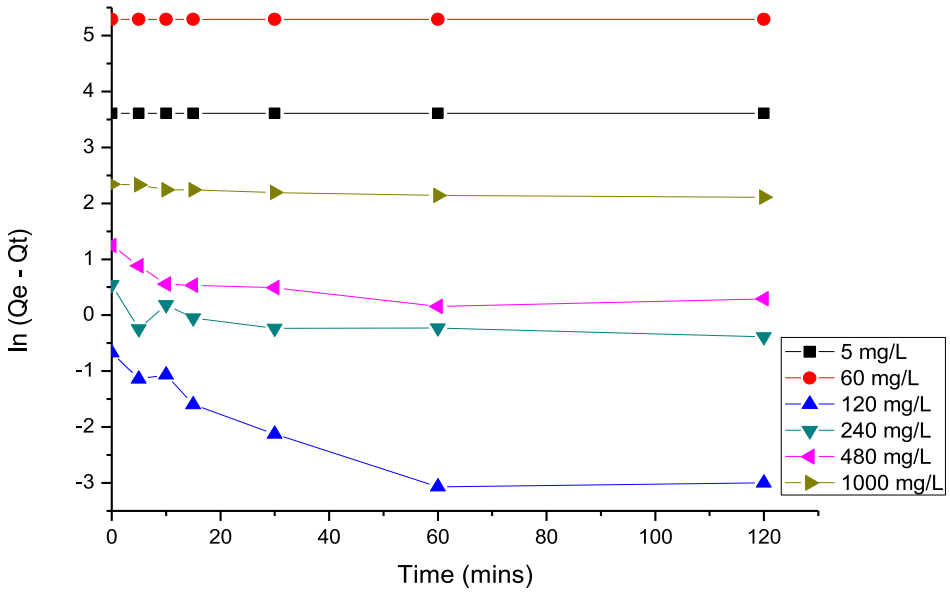

Fig. 8. Fe (II) biosorption by immobilized algal beads: a pseudo-first-order kinetic model.

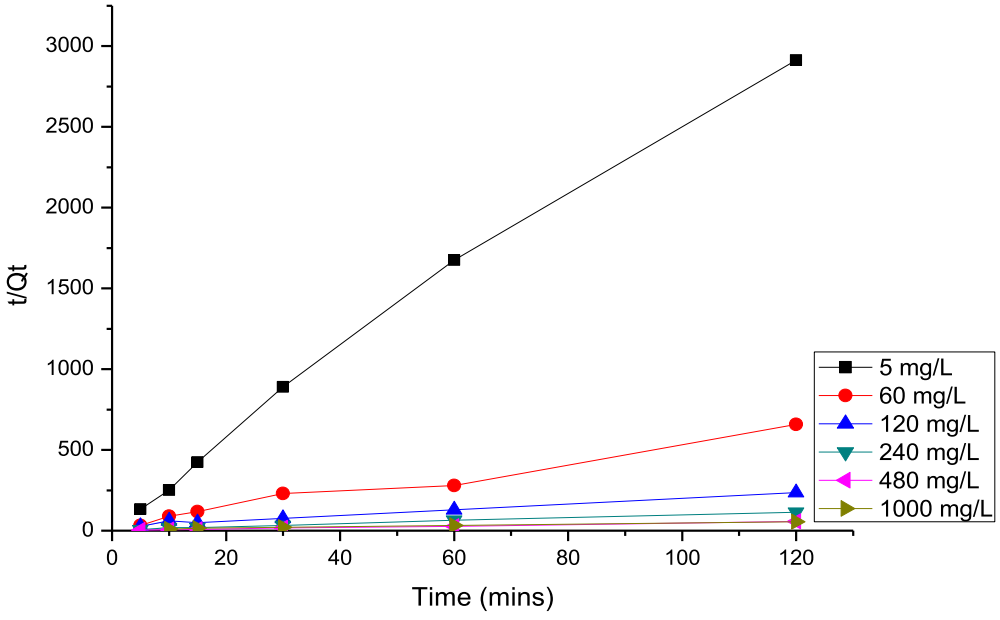

Fig. 9. Fe (II) biosorption on pseudo-second-order kinetics by immobilized algal beads.

min). Integrating this for the boundary conditions $t = 0$ to $t = t$ and $q_t = 0$ to $q_t = q_t$, Eq. (19) may be rearranged for linearized data plotting as shown by Eq. (20):

$$\log(q_e - q_t) = \log(q_e) - \frac{k_1}{2.303}t \quad (20)$$

A plot of log (q_e _ q_t) against t, gives a straight line and q_e and k_1 can be calculated from the slope and intercept, respectively. The pseudo-second-order equation is not based on the concentration of solution like the pseudo-first-order, but on sorption equilibrium capacity (Ho and McKay, 1998;1999) and is expressed as (Eq. (21)):

$$\frac{dq_t}{d_t} = k_2(q_e - q_t)^2 \quad (21)$$

Integrating Eq. (21) gives rise to Eq. (22):

$$\frac{t}{q_t} = \frac{1}{k_2 q_e^2} + \frac{1}{q_e}t \quad (22)$$

Where: q_e and q_t are the sorption capacities at equilibrium and at the time, respectively (mg/g). k_2 is the pseudo-second-order rate constant [g/ (mg/min)]. A plot of $\frac{t}{q_t}$ vs t, gives a straight line. The slope can be used to determine the sorption at equilibrium, and the intercept can be used to determine the rate constant. The biosorption kinetics of Fe (II) ions at a variety of starting concentrations, including 5, 60, 120, 240, 480 and 1000 mg/L, were examined using the pseudo-first-order and pseudo-second-order kinetic models. The model parameters, which are also listed in Table 3, are shown in Figs. 8 and 9. For initial Fe (II) concentrations of 5, 60, 120, 240, 480 and 1000 mg/L, the pseudo-first-order R^2 values were 0.18, 0.38, 0.76, 0.41, 0.48 and 0.76, respectively. As the initial concentration of Fe (II) rose in *Desmodesmus sp.*, the reaction rate (k_2) decreased. With the exception of a starting concentration of 1000 mg/L, the correlation coefficient investigation showed that almost all R^2 values for Fe (II) biosorption kinetics for pseudo-second order kinetic equation were less than 0.99. This shows that chemisorption may be the cause of the removal of Fe (II) by IDS. To improve its fit to the experimental data, the second-order rate constants k_2 and Q_{eq} were derived using the slopes and intercepts of the plots in Figs. 8 and 9. The chemisorption rate-liming mechanism, which incorporates valence forces through the sharing or exchange of electrons between the sorbent and sorbate, is the basis for the pseudo-second-order kinetic model.

4. Conclusion

A calcium alginate matrix was used to immobilize *Desmodesmus sp.*, and its ability to remove Fe (II) from aqueous solutions was evaluated. This study has shown that an increase in Fe (II) ion concentration showed a direct increase in the metal biosorption capacity of the biosorbent. The biosorbent's saturation was attained between 480 mg/L and 1000 mg/L, resulting in a maximum loading capability of 2.27 mg/g. This indicates that the biosorbent has a sufficiently high loading capacity and a comparably high Fe (II) removal percent for the remediation of Fe (II) from contaminated water streams. *Based on the findings, the current study showed a direct relationship between the amount of Fe (II) ions and the biosorbent's capacity to bind metals. Desmodesmus sp.* seems to be a promising strain for effective AMD wastewater bioremediation. Biosorption process of Fe (II) metal by mobilized *Based on the findings, the current study showed a direct relaoshp between the amount of Fe (II) ions and the biosorbent's capacity to bind metals. Desmodesmus sp.* followed the pseudo-second-order and kinetic model equations supported this. This is the first study that showed the great potential of acid-tolerant immobilized green microalgae and novel method for iron removal from AMD effluent, thus paving for the green circular economyseems to be a promising strain for effective AMD wastewater bioremediation. Biosorption process of Fe (II) metal by mobilized *Desmodesmus sp.* followed the pseudo-second-order and kinetic model equations supported this. This is the first study that showed the great potential of acid-tolerant immobilized green microalgae and novel method for iron removal from AMD effluent, thus paving for the green circular economy.

Declaration of Competing Interest

The authors declare that they have no known competing financial interests or personal relationships that could have appeared to influence the work reported in this paper.

Acknowledgements

The authors would like to thank the National Research Foundation (AEMD13121658881) (NRF), Canon Collins Trust and Material and Process Synthesis (MaPS) research section at UNISA for their support and excellent administration of funding this research work.

References

Abdullahet, N., Yusof, N., Lau, W.J., Jaafar, J., Ismail, A.F., 2019. Recent trends of heavy metal removal from water/wastewater by membrane technologies. J. Ind. Eng. Chem. 76, 17–38. https://doi.org/10.1016/j.jiec.2019.03.029.

Abidli, A., Huang, Y., Rejeb, Z.B., Zaoui, A., Park, C.B., 2022. Sustainable and efficient technologies for removal and recovery of toxic and valuable metals from wastewater: recent progress, challenges, and future perspectives. Chemosphere 292, 133102. https://doi.org/10.1016/j.chemosphere.2021.133102.

Adhiya, J., Cai, X., Sayre, R.T., Traina, S.J., 2002. Binding of aqueous cadmium by the lyophilized biomass of Chlamydomonas reinhardtii. Colloids Surf. A Physicochem. Eng. Asp. 210, 1–11. https://doi.org/10.1016/S0927-7757(02)00041-9.

Akpan, L., Tse, A.C., Giadom, F.D., Adamu, C.I., 2021. Chemical characteristics of discharges from two derelict coal mine sites in Enugu Nigeria: implication for pollution and acid mine drainage. JME 12, 89–111.

Akpomie, K.G., Dawodu, F.A., 2015. Physicochemical analysis of automobile effluent before and after treatment with an alkaline-activated montmorillonite. J. Taibah. Univ. Sci. 9, 465–476. https://doi.org/10.1016/j.jtusci.2014.10.005.

Alcolea, A., Vázquez, M., Caparrós, A., Ibarra, I., García, C., Linares, R., Rodríguez, R., 2012. Heavy metal removal of intermittent acid mine drainage with an open limestone channel. Miner. Eng. 26, 86–98. https://doi.org/10.1016/j.mineng.2011.11.006.

Al-Qunaibit, M.H., 2004. A kinetic study of uptake of some cationic entities by the alga chlorella vulgaris. Chemindix WTR06.

Aryal, M., Liakopoulou-Kyriakides, M., 2013. Binding mechanism and biosorption characteristics of Fe (III) by Pseudomonas sp. Cells. JWS. 3, 117–131.

Barka, N., Abdennouri, M., Makhfouk, M.E., Qourzal, S., 2013. Biosorption characteristics of cadmium and lead onto eco-friendly dried cactus cladodes. J. Environ. Chem. Eng. 1, 144–149. https://doi.org/10.1016/j.jece.2013.04.008.

Bashir, A., Malik, L.A., Ahad, S., Manzoor, T., Bhat, M.A., Dar, G.N., Pandith, A.H., 2019. Removal of heavy metal ions from aqueous system by ion-exchange and biosorption methods. Environ. Chem. Lett. 17, 729–754. https://doi.org/10.1007/s10311-018-00828-y.

Bhatt, P., Bhandari, G., Turco, R.F., Aminikhoei, Z., Bhatt, K., Simsek, H., 2022. Algae in wastewater treatment, mechanism, and application of biomass for production of value-added product. Environ. Pollut. 309, 119688 https://doi.org/10.1016/j.envpol.2022.119688.

Birungi, Z.S., Chirwa, E.M.N., 2015. The adsorption potential and recovery of thallium using green micro-algae from eutrophic water sources. J. Hazard. Mater. 299, 67–77. https://doi.org/10.1016/j.jhazmat.2015.06.011.

Boudebbouz, A., Boudalia, S., Bousbia, A., Habila, S., Boussadia, M.I., Gueroui, Y., 2021. Heavy metals levels in raw cow milk and health risk assessment across the globe: a systematic review. Sci. Total. Environ. 751, 14183. https://doi.org/10.1016/j.scitotenv.2020.141830.

Briffa, J., Sinagra, E., Blundell, R., 2020. Heliyon. In: Heliyon, 6, p. e04691. https://doi.org/10.1016/j.heliyon.2020.e04691.

Dada, A.O., Olalekan, A.P., Olatunya, A.M., Dada, O., 2012. Langmuir, Freundlich, Temkin and Dubinin–Radushkevich isotherms studies of equilibrium sorption of Zn2 + unto phosphoric acid modified rice husk. J. Appl. Chem. 3, 38–45. https://doi.org/10.9790/5736-0313845.

Davis, T.A., Volesky, B., Mucci, A., 2003. A review of the biochemistry of heavy metal biosorption by brown algae. Water Res 37, 4311–4330. https://doi.org/10.1016/S0043-1354(03)00293-8.

Fu, F., Wang, Q., 2011. Removal of heavy metal ions from wastewaters: a review. J. Environ. Manage. 92, 407–418. https://doi.org/10.1016/j.jenvman.2010.11.011.

Fu, Z., Xi, S., 2020. The effects of heavy metals on human metabolism. Toxicol. Mech. Methods 30, 167–176. https://doi.org/10.2478/intox-2014-0009.

Genty, T., Bussière, B., Potvin, R., Benzaazoua, M., Zagury, G.J., 2012. Dissolution of calcitic marble and dolomitic rock in high iron concentrated acid mine drainage: application to anoxic limestone drains. Environ. Earth Sci. 66, 2387–2401. https://doi.org/10.1007/s12665-011-1463-3.

Ho, Y.S., McKay, G., 1998. A comparison of chemisorption kinetic models applied to pollutant removal on various sorbents. Process Saf. Environ. Prot. 76, 332–340. https://doi.org/10.1205/095758298529696.

Ho, Y.S., McKay, G., 1999. Pseudo-second order model for sorption processes. Process Biochem 34, 451–465. https://doi.org/10.1016/S0032-9592(98)00112-5.
Jaafari, J., Yaghmaeian, K., 2019. Optimization of heavy metal biosorption onto freshwater algae (Chlorella coloniales) using response surface methodology (RSM). Chemosphere 217, 447–455. https://doi.org/10.1016/j.chemosphere.2018.10.205.
Kumar, S.K., Dahms, H.U., Won, E.J., Lee, J.S., Shin, K.H., 2015. Microalgae – a promising tool for heavy metal remediation. Ecotoxicol. Environ. Saf. 113, 329–352. https://doi.org/10.1016/j.ecoenv.2014.12.019.
Leong, Y.K., Chan, J.S., 2020. Bioremediation of heavy metals using microalgae: recent advances and mechanisms. Bioresour. Technol. 303, 122886 https://doi.org/10.1016/j.biortech.2020.122886.
Lichtfouse, E., Schwarzbauer, J., Robert, D. (eds)(2012). Environmental Chemistry For a Sustainable world. Remediation of Air and Water Pollution, 2, p 541. https://doi.org/10.1007/978-94-007-2442-6.
Makhanya, B.N., Nyandeni, N., Ndulini, S.F., Mthembu, M.S., 2021. Application of green microalgae biofilms for heavy metals removal from mine effluent. Phys. Chem. Earth 124, 103079. https://doi.org/10.1016/j.pce.2021.103079.
Maqsood, Q., Hussain, N., Mumtaz, M., 2022. Novel strategies and advancement in reducing heavy metals from the contaminated environment. Arch. Microbiol. 204 https://doi.org/10.1007/s00203-022-03087-2, 478.
Maree, J.P., Streydom, W.F., Adlem, C.J.L., De Beer, M., Van Tonder, G.J., van Dijk, B.J., 2004. Water Research Commission. Pretoria.
Mathur, P., Chakrabarty, D., Hossain, M.M., 1991. Mixed chalcogen carbonyl compounds: III. Construction of the new unsaturated mixed metal clusters Fe2Ru2 (CO)10(μ-CO)(μ4-Se)(μ4-Te) and Fe3Ru(CO)10(μ-CO)(μ4-Te). J. Organomet. Chem. 418, 415–420. https://doi.org/10.1016/0022-328X(91)80226-A.
Mehta, S.K., Gaur, J.P., 2001. Removal of Ni and Cu from single and binary metal solutions by free and immobilized Chlorella vulgaris. Eur. J. Protistol. 37, 261–271. https://doi.org/10.1078/0932-4739-00813.
Mehta, S.K., Gaur, J.P., 2005. Use of algae for removing heavy metal ions from wastewater: progress and prospects. Crit. Rev. Biotechnol. 25, 113–152. https://doi.org/10.1080/07388550500248571.
Monteiro, C.M., Marques, A.P.G.C, Castro, P.M.L., Malcata, F.X., 2009. Characterization of Desmodesmus pleiomorphus isolated from a heavy metal-contaminated site: biosorption of zinc. Biodegradation 20, 629–641. https://doi.org/10.1007/s10532-009-9250-6.
Pathak, P., Choppin, G., 2009. Effects of pH, ionic strength, temperature and complexing anions on the sorption behaviour of cobalt on hydrous silica. Soil Sediment. Contam. 5, 590–602. https://doi.org/10.1080/15320380903085709.
Plöhn, M., Escudero-Oñate, C., Funk, C., 2021. Biosorption of Cd (II) by Nordic microalgae: tolerance, kinetics, and equilibrium studies. Algal Res 59, 102471. https://doi.org/10.1016/j.algal.2021.102471.
Priyadarshani, I., Sahu, D., Rath, B., 2011. Microalgal bioremediation: current practices and perspectives. J. Biochem. Technol. 3, 299–304.
Réka, H., 2014. Bioremediation of Heavy Metals By Using the Microalga Desmodesmus subspicatus. Bachelor's thesis. Ostfalia University of Applied Sciences.
Rugnini, L., Costa, G., Congestri, R., Antonaroli, S., Sanità di Toppi, L., Bruno, L., 2018. Phosphorus and metal removal combined with lipid production by the green microalga Desmodesmus sp.: an integrated approach. Plant Physiol. Biochem. 125, 45–51. https://doi.org/10.1016/j.plaphy.2018.01.032.
Santaeufemia, S., Abalde, J., Torres, E., 2021. Efficient removal of dyes from seawater using as biosorbent the dead and living biomass of the microalga Phaeodactylum tricornutum: equilibrium and kinetics studies. J. Appl. Phycol. 33, 3071–3090. https://doi.org/10.1007/s10811-021-02513-0.
Schnee, L.S., Knauth, S., Hapca, S., Otten, W., Eickhorst, T., 2016. Analysis of physical pore space characteristics of two pyrolytic biochars and potential as microhabitat. Plant Soil 408, 357–368. https://doi.org/10.1007/s11104-016-2935-9.
Schultz, J., Muller, T., Achtziger, M., Seibel, P.N., Dandekar, T., Wolf, M., 2006. The internal transcriber spacer 2 database-a web server for (not only) low level phylogenetic analyses. Nucleic Acids Res 34, W704–W707.
Seath, S.G., van Niekerk, J.A., 2011. Witwatersrand gold fields: acid mine drainage (Phase 1). BKS Report no.: J01599/05.
Shen, N., Chirwa, E.M.N., 2018. Equilibrium and kinetic modeling for biosorption of Au (III) on freshwater microalgae. J. Appl. Phycol. 30, 3493–3502. https://doi.org/10.1007/s10811-018-1479-1.
Tarawou, T., Wankasi, D., Horsfall, M., 2010. Sorption kinetic study on the removal of basic blue-9 dye using activated carbon produced from water spinach. Int. J. Biol. Chem. Sci. 4, 703–709. https://doi.org/10.4314/ijbcs.v4i3.60496.
Taylor, J., Pape, S., Murphy, N., 2005. A summary of passive and active treatment technologies for acid and metalliferous drainage (AMD) 49.
Wang, L.K., Chen, J.P., Hung, Y., Shammas, N.K., 2009. Heavy Metals in the Environment. Taylor & Francis Group, USA.
Wong, Y.&., Yam, N.F.Y., 1998. Wastewater Treatment With Algae. Springer-Verlag Berlin Heildelberg, New York.